Periodic Hartree-Fock linear combination of crystalline orbitals calculation of the structure, equation of state and elastic properties of titanium diboride

2000 J. Phys.: Condens. Matter 12 7205

(http://iopscience.iop.org/0953-8984/12/32/305)

J. Phys.: Condens. Matter **12** (2000) 7205–7222. Printed in the UK PII: S0953-8984(00)13909-8

Periodic Hartree–Fock linear combination of crystalline orbitals calculation of the structure, equation of state and elastic properties of titanium diboride

C A Perottoni†, A S Pereira†‡ and J A H da Jornada§‖

† Instituto de Física, Universidade Federal do Rio Grande do Sul, 91501-970, Porto Alegre—RS, Brazil

‡ Escola de Engenharia, Universidade Federal do Rio Grande do Sul, 91501-970, Porto Alegre—RS, Brazil

§ Inmetro, Instituto Nacional de Metrologia, Normalizačao e Qualidade Industrial, Campus Avancado de Xerém, Rod. Washington Luiz, km 102.5, BR 040, Duque de Caxias—RJ, Brazil

Received 15 May 2000

Abstract. We have performed all-electron *ab initio* calculations for TiB_2 in the athermal limit using the CRYSTAL95 code. The lattice parameters of the AlB_2-type structure were optimized as a function of pressure. The fitting of a Murnaghan equation of state resulted in values of $B_0 = 292 \pm 1$ GPa and $B'_0 = 3.34 \pm 0.03$ for the bulk modulus and its first derivative at zero pressure. The values for the linear bulk modulus along the a-axis and the c-axis are $B_{a0} = 1031 \pm 3$ GPa ($B'_{a0} = 10.6 \pm 0.2$) and $B_{c0} = 675 \pm 3$ GPa ($B'_{c0} = 8.8 \pm 0.2$), respectively. All five independent elastic constants were calculated, and the analysis of the elastic behaviour of titanium diboride indicates that this compound is more isotropic than one would suppose from its crystal structure. The discussion on the nature of the chemical bonds and the electronic charge transfer in titanium diboride gives some insight into its mechanical properties, such as its high hardness, despite an apparent layered structure. In this sense, the analysis of the charge-density distribution shows a non-negligible interaction between graphite-like boron planes along the c-axis, which increases with pressure, and suggests a three-dimensional picture for the TiB_2 structure, instead of the traditional planar description.

1. Introduction

Since the advent of quantum mechanics in the first decades of this century, one of the biggest challenges in physics has been the development of strategies to overcome the difficulties arising in the calculation of the properties of many-body systems. Nowadays, the availability of sophisticated codes and powerful computers has made it entirely possible to undertake *ab initio* computer experiments. Among the many fields in condensed matter physics where this approach can be exploited, we have particular interest in the study of the pressure behaviour of very hard materials. Usually, extremely high pressures are needed for the study of such materials in order to induce some significant change in their structures. At such high static pressures, the production of hydrostatic conditions is not always possible and the samples are necessarily very small. This imposes many restrictions on the kind and precision of the analytical techniques which can be used to extract information from the sample under pressure.

‖ On leave from: Instituto de Física, Universidade Federal do Rio Grande do Sul, 91501-970, Porto Alegre—RS, Brazil.

0953-8984/00/327205+18$30.00

In such a context, carrying out complementary computer experiments is very convenient, in at least two respects: they enable us to 'process' a material under conditions that are sometimes hard to reproduce experimentally; and they can give us some insight into the actual behaviour observed in real experiments.

Titanium diboride is a material which presents a very attractive combination of mechanical, chemical and transport properties such as high hardness (from 20 to 30 GPa at room temperature, depending on the applied load), high melting point (about 3500 K), low density (4495 kg m^{-3}), low electrical resistivity (0.13 $\mu\Omega$ m), good thermal conductivity (ranging from 37 to 122 W m^{-1} K^{-1}, at 300 K) and excellent chemical inertness [1–5]. These characteristics make it a potential candidate for several high-performance applications, in cutting tools, electrodes and wear-resistant components [1–3]. Just for comparison, an excellent thermal and electric conductor such as copper, with a density of 8960 kg m^{-3} (about twice that of TiB_2), has an electrical resistivity of 0.017 $\mu\Omega$ m and a thermal conductivity of 398 W m^{-1} K^{-1} at 300 K [4].

Despite the prominence that TiB_2 has found in high-technology applications, some of its physical properties are scarcely known. For example, to our knowledge there is no published experimental result for the pressure dependence of the TiB_2 lattice parameters and unit-cell volume. Consequently, the TiB_2 bulk modulus is usually obtained by measuring the sound propagation velocity along different axes for TiB_2 single or polycrystalline samples. However, high-purity, large and defect-free single crystals of TiB_2 are difficult to prepare and, consequently, the measurement of the elastic constants is complicated by the small size of the samples employed in the ultrasonic experiments. Another source of difficulties found by experimentalists arises from the existence in the Ti–B phase diagram of a stability field for non-stoichiometric phases TiB_x with $x \approx 2$ [3]. These factors, along with the difficulty of obtaining fully densified polycrystalline samples, could possibly account for the spread observed in the literature for several physical properties of titanium diboride.

Titanium diboride crystallizes in the AlB_2 structure—space group $P6/mmm$, with one titanium at the origin and two boron atoms at the site 2d $(1/3, 2/3, 1/2)$—see figure 1. Its structure is usually described as a simple stacking of graphite-like parallel sheets of boron intercalated with a simple hexagonal lattice of titanium, disposed in such a way that each titanium is surrounded by twelve borons, and each boron is coordinated by six Ti atoms. Although topologically correct, this simple two-dimensional picture can hardly account for the mechanical properties of TiB_2 (and that of the transition-metal diborides in general), such as its high strength and hardness.

There are several theoretical studies in the literature, involving different approaches, whose main concern is the electronic structure of the transition-metal diborides, in particular those with the AlB_2 structure [6–13]. However, only a few of them concern the pressure behaviour and elastic properties of these compounds. Among these, we must cite in particular van Camp and van Doren [13], who performed density functional calculations (in both local density (LDA) and generalized gradient (GGA) approximations) for TiB_2. In their work, van Camp and van Doren imposed a second-order polynomial expression for the energy dependence on the lattice parameters, and fitted its coefficients to forty-two points on the *ab initio* energy hypersurface. In our paper we will follow a different approach, in that the total energy is evaluated directly *ab initio*, each time we need it. Moreover, despite the approximate inclusion of correlation effects in DFT clearly giving better estimates for binding energies, the same is not always true for other physical properties that depend on energy derivatives. It seems also that the exact treatment of exchange in the Hartree–Fock approximation is of primary importance in the description of the electronic charge distribution of covalent solids [14]. This particular advantage of HF theory over DFT will prove to be of great value for the

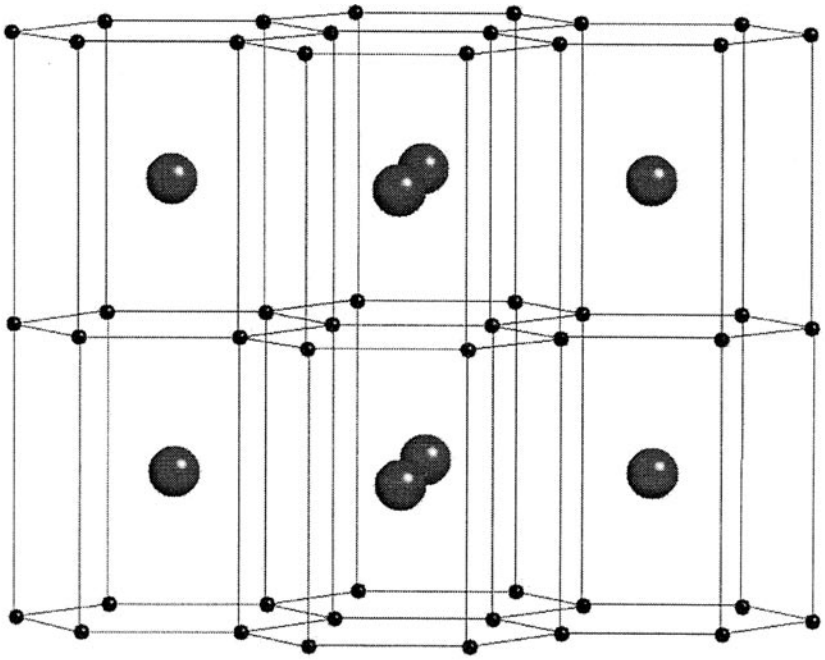

Figure 1. TiB_2 crystal structure. Large and small spheres represent titanium and boron atoms, respectively.

understanding of the effect of the interaction between boron planes on the elastic properties of TiB_2.

In this context, in this paper we provide a set of physical properties for titanium diboride, calculated from first principles within the Hartree–Fock mean-field approximation. Our findings are compared with other theoretical and experimental results, in order to assess the relative merits of our approach. The main intent of this work is to provide a coherent picture for the mechanical and bonding properties of TiB_2, based on the analysis of its elastic behaviour and electronic charge-density distribution.

This paper is organized as follows. In section 2 we present the computational procedure and the basis sets used to undertake the calculations. Section 3 presents the results obtained for the equilibrium geometry and equation of state for TiB_2 at $T = 0$. In section 4 we deal with the calculation of the single-crystal elastic constants and the Hill averages of the elastic moduli for an isotropic, homogeneous polycrystalline aggregate of titanium diboride. The results obtained are discussed and compared with other theoretical and experimental results available in the literature. Electronic charge-distribution maps for TiB_2 are shown in section 5, where we discuss some aspects regarding chemical bonding and its influence on the mechanical properties of titanium diboride. Finally, in section 6 we present the main conclusions of this work.

2. Computational details

The all-electron *ab initio* periodic Hartree–Fock calculations were performed with the CRYSTAL95 code [15, 16]. The crystalline orbitals used as the basis for the wavefunction expansion were constructed from a linear combination of atom-centred Gaussian orbitals (HF-LCCO approximation). An 86-4113G basis set was chosen for titanium. The initial exponents

and coefficients for this basis set were taken from Saunders [17]. The exponents and contraction coefficients of the valence orbitals were further optimized by minimizing the total energy for crystalline TiB_2†. The optimal exponent of the outermost titanium 5sp orbital could not be found by minimizing the total energy of the crystalline compound, as the energy decreases monotonically with the sp exponent until a numerical catastrophe occurs [15]. Consequently, the adopted value represents a compromise between numerical convergence, minimal total energy and the computational resources needed to undertake the calculations. The resulting titanium basis set used in this work is given in table 1. For boron, the basis set used was the standard 6-21G, with the external sp exponent set to 0.19 [18]. All the calculations were performed in the athermal limit. To ensure convergence and high numerical accuracy, very tight tolerances were employed in the evaluation of the infinite Coulomb and exchange series: 10^{-8} for the exchange overlap, Coulomb overlap, Coulomb penetration and the first exchange pseudo-overlap; and 10^{-14} for the second exchange pseudo-overlap tolerance [15]. The Fock matrix has been diagonalized at 133 k-points within the irreducible Brillouin zone, corresponding to a shrinkage factor of 12 in the Monkhorst net [19]. Owing to the metallic character of TiB_2, a dense Gilat net [20] was defined with a total of 793 k-points in reciprocal

† The valence exponents and contraction coefficients were optimized by sequential line minimization, with a Unix script shell developed by M Towler (see http://www.tcm.phy.cam.ac.uk/˜mdt26/).

Table 1. The titanium basis set. Exponents (in au) and coefficients of the s, p and d Gaussian functions.

		Coefficients		
Type	Exponent	s	p	d
s	228000.0000	0.000228		
	32450.0000	0.001929		
	6888.6000	0.011100		
	1802.4000	0.049990		
	543.2000	0.170100		
	187.4400	0.369160		
	73.1900	0.402700		
	30.4500	0.144500		
sp	553.4000	−0.005460	0.00853	
	132.1800	−0.070400	0.06021	
	43.6100	−0.117700	0.21330	
	17.0200	0.245100	0.38710	
	7.2600	0.670800	0.40210	
	2.3760	0.286000	0.23900	
sp	28.3000	0.002700	−0.02710	
	11.2400	−0.151500	−0.07670	
	4.6560	−0.744000	0.16650	
	1.8650	1.032000	1.31400	
sp	0.7138	1.000000	1.00000	
sp	0.1500	1.000000	1.00000	
d	6.0511			0.1161
	1.4468			0.3429
	0.3267			0.5250

space, corresponding to a shrinkage factor of 24. In order to reduce the numerical noise, all the calculations were performed with the same set of indexed bielectronic integrals selected from a reference geometry [15]. To improve the convergence, the Fock matrix (F_i^{new}) at the self-consistent-field cycle i was made equal to

$$F_i^{new} = (1 - p)F_i + pF_{i-1} \tag{1}$$

where p is a mixing parameter equal to 0.3 [15]. In general, some 20 to 30 SCF cycles were sufficient to achieve convergence in total energy to within 10^{-6} to 10^{-8} Hartree per primitive cell. A further increase in the cut-off for the evaluation of bielectronic integrals as well as in the shrinkage factors that define the Monkhorst and Gilat nets resulted in changes in the total energy smaller than 1 mHartree.

3. TiB_2 equilibrium geometry and equation of state

The total HF energy of TiB_2 was minimized as a function of the hexagonal lattice parameters using the conjugate-gradient algorithm of Polak and Ribiere [21]. No constraints were imposed on the c/a ratio, i.e., both lattice parameters were optimized simultaneously. As can be seen in table 2, the resulting lattice parameters a and c are in excellent agreement with the experimental values, differing from those of Post *et al* [22] by -0.1% and 0.3%, respectively. No correction was made to account for the temperature effect on the lattice parameters, which should be almost negligible in any case.

Table 2. Lattice parameters, bulk moduli (B_0) and pressure derivatives (B_0') of titanium diboride at zero pressure.

Reference	a_0 (Å)	c_0 (Å)	V_0 (Å^3)	B_0 (GPa)	B_0'	B_{iso} (GPa)
Experimental[a]						
Silver and Kushida [24]	3.028	3.228	25.6			
Post *et al* [22]	3.030	3.230	25.7			
Gilman and Roberts [25]				399		436
Spoor *et al* [26]				240		247
Manghnani *et al* [27]				239		240
Wright[b]				194		239
Wright[c]				237		253
Theoretical						
This work	3.027	3.240	25.7	292	3.34	
This work[d]				299		306
Van Camp and van Doren[e]	3.023	3.166	25.1	270		273
Van Camp and van Doren[f]	2.993	3.147	24.4	260		260
Tian and Wang [6]	2.895	3.086	22.4			377

[a] Bulk modulus calculated from measured single-crystal elastic constants.
[b] Bulk modulus calculated from the Voigt estimate of the single-crystal elastic constants [28].
[c] The same as above, but in the Reuss approximation.
[d] As calculated from the elastic constants given in table 3, later.
[e] Density functional theory (DFT) with *ab initio* norm-conserving pseudopotentials in the local density approximation (LDA) for the exchange–correlation contribution to the energy [13].
[f] The same as above, but in the generalized gradient approximation (GGA).

In order to provide some insight into the pressure behaviour of TiB_2, the HF energy of titanium diboride was minimized as a function of the c/a ratio for selected values of the primitive-cell volume. The dependence of the HF energy (E) on the volume of the TiB_2

primitive cell can be seen in figure 2(a). The solid curve in figure 2(a) represents the fitted Murnaghan equation of state:

$$E = E_0 + \frac{B_0}{B_0'}(V - V_0) - \frac{B_0 V_0}{B_0'(1 - B_0')}\left[\left(\frac{V}{V_0}\right)^{1-B_0'} - 1\right] \tag{2}$$

where V is the primitive-cell volume, B is the bulk modulus and B' its first pressure derivative. The zero index means the values at zero pressure. The fitting yielded $B_0 = 292 \pm 1$ GPa, $B_0' = 3.34 \pm 0.03$ and $V_0 = 25.8$ Å^3. The quoted uncertainties refer to the standard deviation of the fitted parameters. These values are compared in table 2 with those derived from single-crystal elastic constants and other theoretical estimates taken from the literature.

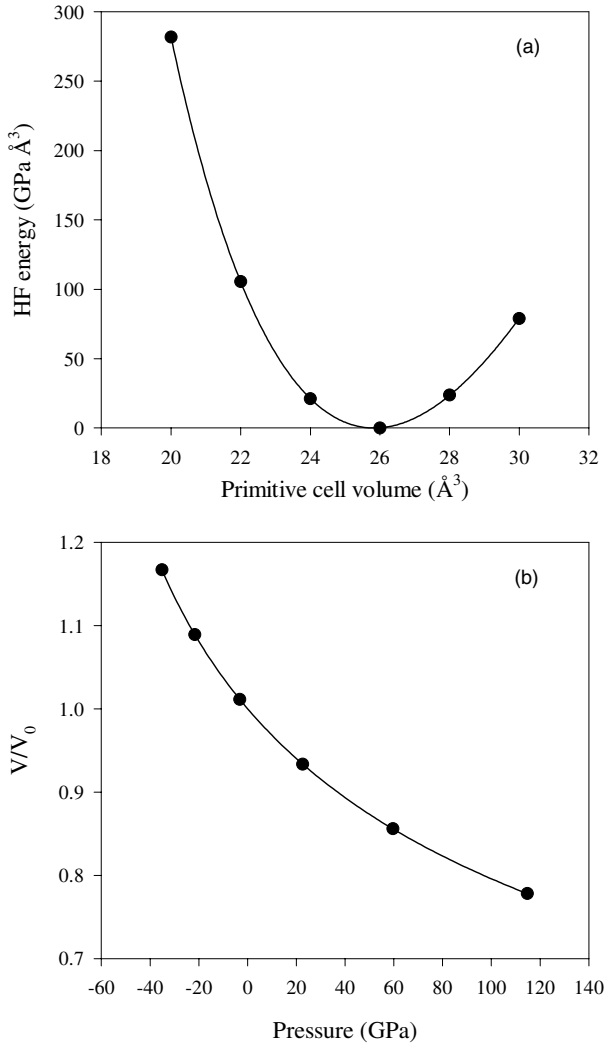

Figure 2. (a) TiB_2 HF energy as a function of the primitive-cell volume. The solid curve is the resulting fit of the Murnaghan equation of state (2). (b) The pressure dependence of the TiB_2 primitive-cell volume. The solid curve represents the Murnaghan equation (3) with the parameters taken from the fitting in (a).

The primitive-cell equilibrium volume at zero pressure agrees within 0.1 Å^3 with the value obtained from the unconstrained optimization of the TiB_2 structure (see table 2), revealing the consistency of our calculations and the adequacy of the Murnaghan equation of state.

From equation (2), the pressure acting on the system as a function of the primitive-cell volume can be obtained through the thermodynamic relationship

$$P(V) = -\frac{dE}{dV} = \frac{B_0}{B_0'}\left[\left(\frac{V_0}{V}\right)^{B_0'} - 1\right]. \tag{3}$$

The resulting pressure dependence of the TiB_2 primitive-cell volume is shown in figure 2(b).

With the pressure calculated according to equation (3) and the optimized hexagonal c/a ratio at each volume, we obtained the pressure dependence of the titanium diboride lattice parameters, as shown in figure 3. The linear bulk modulus at zero pressure B_{a0} and B_{c0}, i.e., the inverse linear compressibility along the crystallographic axis, under isotropic stress, and their pressure derivatives, were obtained by fitting the Murnaghan equation (3) to the points in figure 3(a). Proceeding in this way, the values obtained were $B_{a0} = 1031 \pm 3$ GPa ($B_{a0}' = 10.6 \pm 0.2$) and $B_{c0} = 675 \pm 3$ GPa ($B_{c0}' = 8.8 \pm 0.2$). Both TiB_2 linear bulk moduli rapidly increase with pressure, despite B_c always being smaller than B_a in the pressure range up to 115 GPa. The extremely high linear bulk modulus parallel to the boron planes has a magnitude comparable to that of the carbon planes in graphite, namely $B_{a0} = 1250$ GPa (with fixed $B_{a0}' = 1$) [23]. Indeed, the TiB_2 linear bulk modulus B_a will become even greater than that of a hypothetical graphite structure at pressures above 23 GPa (single-crystalline samples of graphite are stable just up to 14 GPa [23]). The TiB_2 linear bulk modulus B_{c0} is one order of magnitude higher than that of graphite, a true layered structure. In section 5 it will be shown that the charge-density analysis for TiB_2 can shed some light on these interesting results.

The equilibrium lattice parameters resulting from the fitting of the Murnaghan equation (3) to the points in figure 3(a), $a_0 = 3.019$ Å and $c_0 = 3.257$ Å, differ by -0.26% and 0.52%, respectively, from the values obtained by unconstrained structure optimization, as quoted in table 2.

4. Elastic properties

The five independent elastic constants of titanium diboride were calculated by imposing a set of different deformations on the hexagonal lattice and following the dependence of the primitive-cell energy on the applied strain. The lattice deformations employed here were those suggested by Fast, Wills, Johansson and Erikson [29]. They were chosen in such a way that the second-order term in the expansion of the strain energy as a function of the adimensional deformation parameter ε could be related to a particularly simple combination of the elastic constants. The atomic coordinates were not optimized each time the lattice was distorted. This should not affect the result for $c_{11} + c_{12}$ and c_{33}, as the site symmetries and the Bravais lattice remain unchanged for the particular lattice deformation involved in their estimate. On the other hand, the effect of the residual inner stress on the other elastic constants should not be greater than about 10% of the calculated values, as can be inferred from previous results in the literature (see, e.g., the results for MgF_2 [30]). The dependence of the strain energy on ε is shown in figure 4, for the five distinct lattice deformations. To reduce the influence of high-order terms in the expansion of the strain energy, the maximum deformation amounts to $\pm 2\%$ of the equilibrium lattice parameters. Third-order polynomials were fitted to the data in figure 4, from which the elastic constants of TiB_2 were calculated according to equations (6) to (15) of reference [29]. The effect of introducing high-order terms in the polynomial fitting was negligible. The results are given in table 3. A further reduction of the maximum lattice deformation did not

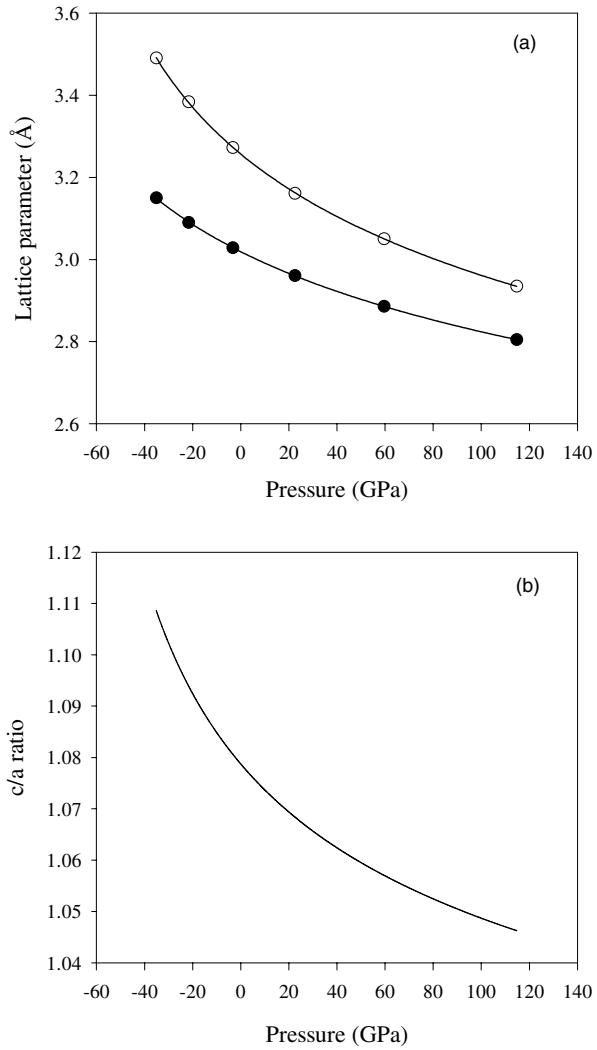

Figure 3. (a) The pressure dependence of the TiB_2 lattice parameters a (full circles) and c (open circles). (b) The c/a ratio as a function of pressure. The solid curves in (a) show the fitting of the Murnaghan equation (3) for the lattice parameters.

result in elastic constants significantly different from those quoted in table 3. The deviation from zero deformation of the minimum in the energy curve for the calculation of c_{33}, seen in figure 4, just means that the algorithm used to search for the structure of minimum energy was not exhaustively iterated. In any case, the correction for the lattice parameters, owing to this observed deviation, should amount to only about 0.5%.

Among the five elastic constants of TiB_2, the value of c_{44} was particularly difficult to obtain, since its calculation involves a triclinic deformation of the hexagonal unit cell, increasing by a factor of four the number of points needed to interpolate the wavefunction in the irreducible Brillouin zone (keeping a shrinkage factor of 12 in the Monkhorst net).

Despite the large discrepancies between the reported experimental single-crystal elastic constants for TiB_2, the analysis of the data in table 3 can reveal some trends in our results.

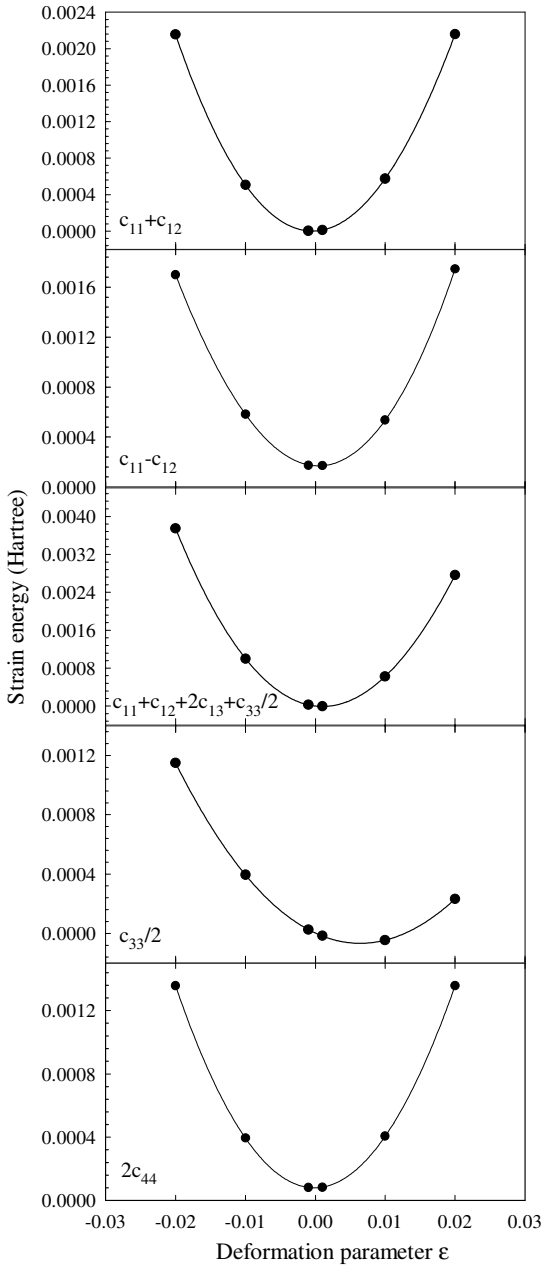

Figure 4. The dependence of the strain energy on the adimensional lattice deformation parameter ε. The inset in each panel shows the specific combination of elastic constants in the second-order term of the $E(\varepsilon)$ expansion, from which the elastic constants were obtained [29].

There is a good agreement between our values for c_{13} and c_{33} and those calculated by van Camp and van Doren [13]. On the other hand, the value obtained by them for $c_{11} + c_{12}$ is between 15 and 20% (depending on the particular functional used for the exchange–correlation contribution to energy) smaller than our result. Our estimates for the elastic constants c_{13} and

Table 3. Elastic constants of titanium diboride (GPa).

Reference	c_{11}	c_{12}	c_{13}	c_{33}	c_{44}
Experimental					
Gilman and Roberts [25]	690	410	320	440	250
Spoor *et al* [26]	660	48	93	432	260
Manghnani *et al*[a]	588	72	84	503	238
Wright[b]	672	40	125	224	232
Wright[c]	711	17	118	349	240
Theoretical					
This work	786	127	87	583	271
Van Camp and van Doren[d]	777[e]		83	568	
Van Camp and van Doren[f]	730		78	572	

[a] TiB_2 polycrystalline elastic stiffnesses [27].
[b] Voigt estimates of the single-crystal elastic constants calculated from the reported values of Manghnani, Fisher, Li and Grady [27] after correction for texture effects [28].
[c] The same as above, but using the Reuss approximation.
[d] DFT with *ab initio* norm-conserving pseudopotentials in the local density approximation (LDA) for the exchange–correlation contribution to the energy [13].
[e] $c_{11} + c_{12}$.
[f] The same as in note d, but in the generalized gradient approximation (GGA).

c_{44} of TiB_2 compare well with the values measured at room conditions by Spoor *et al* [26]. The agreement is worse for c_{11}, c_{33} and c_{12}. However, one should note the great variance among the experimental results, mainly for c_{12}. The DFT value for $c_{11} + c_{12}$ is closer to the experimental results than the corresponding HF estimate of this work. However, both HF and DFT (in the LDA and GGA approximation) approaches lead to a value for c_{33} somewhat greater than the experimental one. This tendency of HF calculations to overestimate some elastic constants was already pointed out by several authors (see, e.g., references [30–32]).

From the general relationship between elastic compliances (s_{ij}) and bulk compressibility [33]

$$\frac{1}{B} = s_{11} + s_{22} + s_{33} + 2(s_{12} + s_{23} + s_{31}) \tag{4}$$

one obtains the bulk modulus at zero pressure for a single crystal with hexagonal symmetry (without constraints on the c/a dependence on lattice strain) as given by

$$B_0 = \frac{c_{33}(c_{11} + c_{12}) - 2c_{13}^2}{c_{11} + c_{12} - 4c_{13} + 2c_{33}}. \tag{5}$$

With the elastic constants from table 3, the above equation yields $B_0 = 299$ GPa, only 2.4% higher than the value obtained from the fitting of the Murnaghan equation of state to the points in figure 2(a). This reveals that the whole set of calculated elastic constants is consistent with the bulk modulus obtained through the analysis of the volume dependence of the primitive-cell energy, as done in section 3.

The elastic anisotropy of a TiB_2 single crystal can be best appreciated by plotting a tridimensional representation of the directional dependence of Young and linear bulk moduli [33] (figure 5). The surface of revolution representing the directional dependence of the TiB_2 bulk modulus, calculated from the set of elastic constants given in table 3, intercepts the a-axis at 1043 GPa and the c-axis at 700 GPa, in good agreement with the B_{a0}- and B_{c0}-values determined from the pressure dependence of the lattice parameters (section 3).

The Young modulus surface of revolution intercepts the c-axis at 566 GPa and the a-axis at 756 GPa. In other words, the Young modulus parallel to the basal plane is about 30% higher

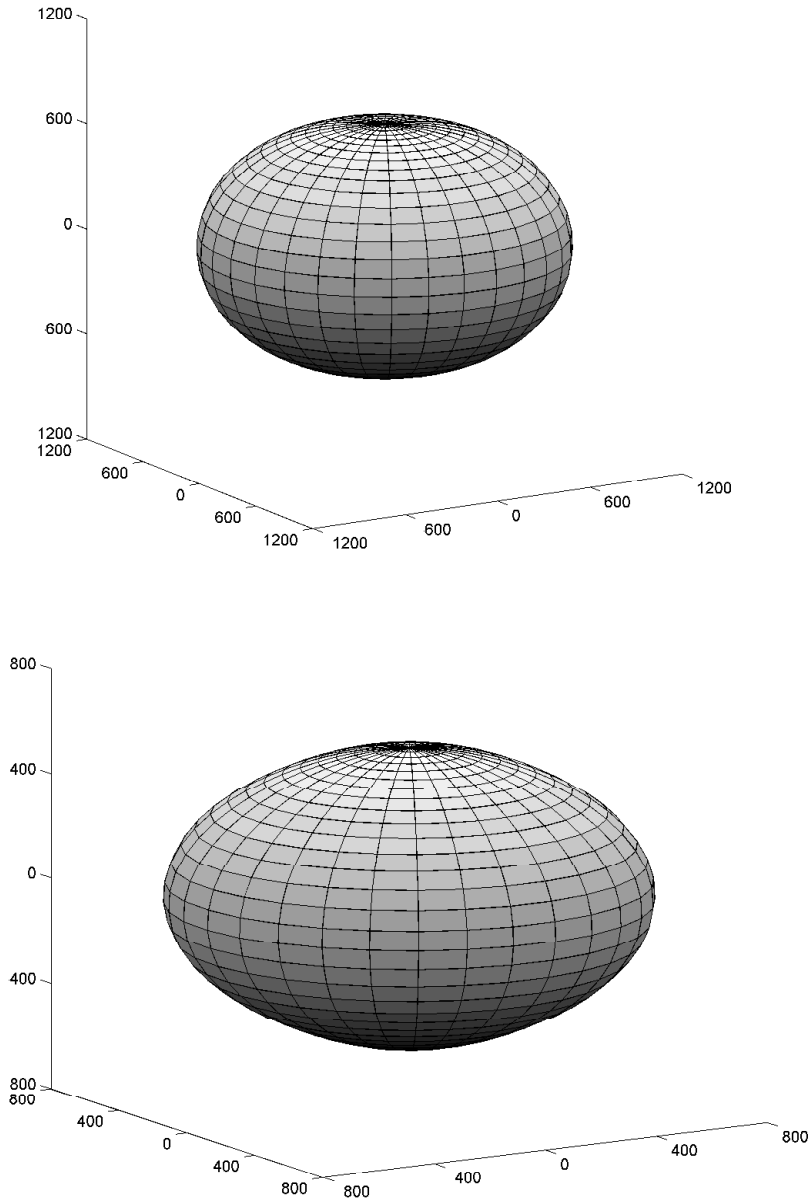

Figure 5. The directional dependency of the bulk (above) and Young (below) moduli of titanium diboride. The axis scales are given in GPa.

than the one parallel to the c-axis. This plot can be directly compared to the experimental results given by Spoor *et al* [26].

The effect of the anisotropic linear compressibility on the overall compressibility of titanium diboride can also be evaluated by calculating the isotropic bulk modulus (B_{iso}), i.e., the bulk modulus obtained under the assumption that the c/a ratio remains unchanged when the lattice is subjected to an isotropic stress. B_{iso} can be written in terms of the elastic

constants as [29]

$$B_{iso} = \frac{2}{9}\left(c_{11} + c_{12} + 2c_{13} + \frac{c_{33}}{2}\right). \tag{6}$$

With our set of elastic constants, the above expression yields $B_{iso} = 306$ GPa, approximately 2.3% above the value obtained from equation (5) when relaxing the c/a ratio. The c/a ratio decreases by only about 2% from ambient pressure to 115 GPa (see figure 3(b)).

There is a substantial amount of experimental work devoted to the determination of the elastic moduli of polycrystalline titanium diboride. To extend the comparison of our results with experiment, the calculated single-crystal elastic constants were used to estimate the averaged elastic moduli of an isotropic polycrystalline aggregate of titanium diboride. In table 4 we report the Hill averages [35] for the Young, shear and bulk moduli, as well as the Poisson ratio for TiB_2. The Hill averages represent the mean value between the Voigt and Reuss bounds on the elastic moduli. Our results are systematically higher than those measured by Wiley, Manning and Hunter, after correction for porosity [26], a consequence of the overestimation of $c_{11} + c_{12}$ and c_{33}. The Poisson ratio agrees well with experiment.

Table 4. Comparison between measured TiB_2 polycrystalline elastic moduli and Hill averages derived from elastic constants. Young (E), shear (G) and bulk (B) moduli are all given in GPa. The Poisson ratio (σ) is adimensional.

Reference	E	G	B	σ
Experimental results with polycrystalline samples				
Abbate, Frankel and Dandekar [37]	549	247	238	0.114
Grady [38]	522	249	193	0.049
Gust, Holt and Royce [36]	541	237	251	0.141
Wiley, Manning and Hunter[a]	505	228	214	0.109
Wiley, Manning and Hunter[b]	568	258	237	0.101
Hill averages from single-crystal elastic constants				
This work	670	296	303	0.132
Gilman and Roberts [25]	447	169	417	0.321
Spoor *et al* [26]	579	262	244	0.105
Wright[c]	539	240	238	0.122

[a] Sample with 6% porosity [34].
[b] The same as above, after correction for porosity [26].
[c] Calculated from the single-crystal elastic constants estimated from the polycrystalline elastic stiffnesses of titanium diboride after correction for texture [28].

One possible measure of the TiB_2 elastic anisotropy is given by the 'percentage anisotropies' in the compressibility and shear [26]. These quantities, defined as

$$A^*_{comp} = \frac{B_V - B_R}{B_V + B_R} \tag{7}$$

and

$$A^*_{shear} = \frac{G_V - G_R}{G_V + G_R} \tag{8}$$

range from zero (perfect elastic isotropy) to 100%, the maximum anisotropy. In the above expressions, B and G are the bulk and shear moduli, as estimated from the Voigt (subscript V) and Reuss (subscript R) approximations. The 'percentage anisotropies' for titanium diboride, as derived from our set of calculated elastic constants, are given in table 5, where they are compared to the values calculated from the single-crystal elastic constants measured by Gilman

Table 5. Percentage anisotropy in the compressibility and shear for titanium diboride.

	Percentage anisotropy	
Reference	A^*_{comp} (%)	A^*_{shear} (%)
This work	1.3	0.7
Gilman and Roberts [25]	4.4	6.3
Spoor *et al* [26]	1.3	1.5

and Roberts [25] and Spoor *et al* [26]. As can be seen, a fair agreement is observed with the results of Spoor *et al*, supporting their conclusion that TiB_2 is more isotropic than previously supposed.

The analysis of the directional dependence of Young and bulk moduli (figure 5), the comparison between fully relaxed and isotropic bulk moduli, as well as the 'percentage anisotropies' given in table 5, all suggest that titanium diboride is much more isotropic than one would suppose exclusively on the basis of the usual description of its 'planar' crystal structure. In fact, it seems that the interactions between boron planes are not negligible at all and must be taken into account in order to better understand the origin of the mechanical properties of TiB_2. In section 5, it will be shown how electronic charge-density maps give support to this interpretation.

5. Electronic charge-density maps

From the crystal structure of TiB_2 depicted in figure 1, one could expect to find a substantial non-uniformity in the bonding properties. This anisotropy can be appreciated in figure 6. The bonding between in-plane boron atoms is strongly covalent, as evidenced by the maximum in the charge density at the bond middle point (figure 6(a)). Such localized bonding is not evident in the plane occupied by titanium. In contrast, the metallic character of the titanium planes can be appreciated in figure 6(b), which shows the titanium cores immersed in a sea of charge-density difference of about 0.005 e Bohr^{-3}.

A charge transfer from the neighbourhood of the titanium atoms is clearly seen in figure 6(c), which maps the charge-density difference in the plane 110. Another feature of interest in this figure is the charge build-up along the line joining boron atoms in adjacent planes. As can be seen in figure 6(d), as pressure increases to 115 GPa, there is also an increasing of the charge transfer from the region between titanium atoms to an envelope of charge around boron atoms and also to a bimodal charge density accumulating between boron planes.

Any particular criterion for the partition of the electronic charge among the components of a polyatomic system—a solid, in this case—will imply some degree of arbitrariness. For instance, the Mulliken population analysis [41], in particular, can yield very different results depending, for instance, on small changes in the basis set employed in the calculations [39,40]. In spite of that, we show in table 6 and table 7 the results of a Mulliken population analysis, including both valence shell and bond-overlap populations for TiB_2 at several pressures, as a complement to the electronic charge-density maps of figure 6. The Mulliken net charges for titanium and boron atoms at ambient pressure in TiB_2 are equal to $q_{\mathrm{Ti}} = 0.376$ and $q_{\mathrm{B}} = -0.188$, suggesting a charge transfer from titanium to boron. This result is in accordance with a recent experimental finding confirming charge transfer from metal to boron in a similar compound, namely TaB_2 [42], and also with other theoretical results, such as those of Tian and Wang [6] and Mizuno *et al* [43].

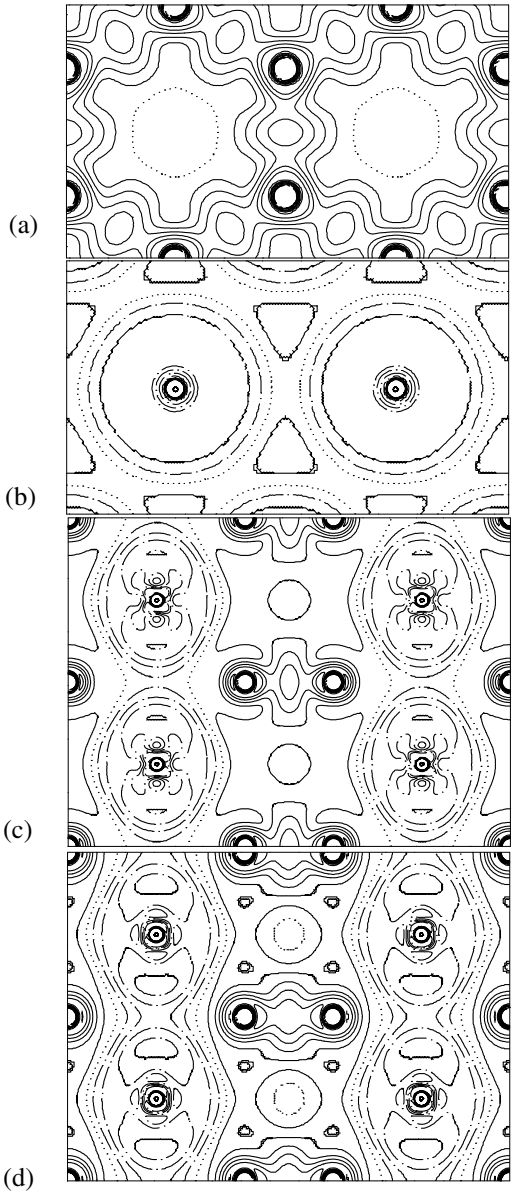

Figure 6. Charge-density difference maps. From the top to the bottom: planes parallel to the basal plane, (a) occupied by boron and (b) by titanium, and plane 110, perpendicular to (a) and (b), containing both titanium and boron atoms, (c) at zero pressure and (d) at 115 GPa. The contour lines are drawn at intervals of 5×10^{-3} e Bohr^{-3}. Continuous, dotted and dot–dash curves correspond to positive, zero and negative charge density relative to a pure superposition of atomic charge densities. (These figures can be seen as colour maps at http://www.if.ufrgs.br/~perott/tib2.htm. At this site there is also an animation illustrating the effect of pressure on the TiB_2 charge-density distribution.)

Our results agree with the experimental charge-density distribution reported by Will and Kirfel [44] as regards a charge excess at the middle point between in-plane boron atoms. However, the charge-density maps in figure 6 differ qualitatively, in at least one respect, from

Table 6. Dependency on pressure of the Ti and B net charge and valence shell population in TiB_2.

	Ti				B		
P (GPa)	q_{Ti} ($\|e\|$)	4sp	5sp	3d	q_B ($\|e\|$)	2sp	3sp
−21.7	0.492	4.757	1.729	2.105	−0.246	1.456	1.792
−3.22	0.396	4.746	1.762	2.175	−0.198	1.533	1.667
0	0.376	4.745	1.768	2.189	−0.188	1.542	1.648
22.6	0.280	4.734	1.803	2.259	−0.140	1.619	1.523
59.6	0.140	4.719	1.854	2.360	−0.070	1.713	1.359
115	−0.030	4.701	1.919	2.480	0.015	1.818	1.169

Table 7. Variation with pressure of the bond-overlap population in TiB_2. Distances between atoms are quoted in ångströms. B′ and Ti′ stand for out-of-plane boron and titanium, respectively.

P (GPa)	Ti–Ti	d_{Ti-Ti}	Ti–B	d_{Ti-B}	B–B	d_{B-B}	B–B′	$d_{B-B'}$	Ti–Ti′	$d_{Ti-Ti'}$
−21.7	0.057	3.091	0.097	2.459	0.223	1.785	0.005	3.384	0.007	3.384
−3.22	0.059	3.029	0.100	2.395	0.213	1.749	0.006	3.272	0.008	3.272
0	0.058	3.027	0.101	2.383	0.210	1.748	0.007	3.240	0.009	3.240
22.6	0.061	2.961	0.102	2.328	0.202	1.709	0.007	3.161	0.009	3.161
59.6	0.063	2.886	0.102	2.259	0.188	1.666	0.009	3.050	0.009	3.050
115	0.065	2.805	0.101	2.186	0.159	1.619	0.010	2.935	0.007	2.935

those of Will and Kirfel. The Fourier synthesis of the electronic charge-density distribution on the 110 plane, as given in reference [44], shows a charge accumulation concentrated along the B–B bond, with the boron surrounded by a negative charge-density envelope. In contrast, our results show a broad, positive charge-density 'wrapper' around boron, that enlarges with pressure, as can be seen in figure 6(d). This positive charge density around boron actually overflows along the *c*-axis, bridging the gap between the boron layers with a continuous, bimodal excess of electronic charge, running directly along the B–B lines perpendicular to the basal plane, and not half-way between each pair of B atoms, as suggested in reference [44]. It is important to remark that both our results and those of Will and Kirfel show a non-negligible interaction along the *c*-axis between stacking borons, a finding contrary to the usual assumption of a 'planar' structure for TiB_2. As the result of DFT calculations, van Camp and van Doren [13] found a fairly uniform charge density between the basal planes of titanium diboride. They did not reported any feature pointing to a particular interaction between boron planes, in contradiction with our results. In this respect, it was recently shown that the exact treatment of exchange in HF approximation is of primary importance in the description of the charge build-up at the middle point of covalent bonds [14]. Consequently, it is not surprising that the bimodal charge accumulation along the line joining boron atoms from adjacent planes was not revealed by previous DFT calculations, in which exchange was taken into account only approximately. Without some degree of directional bonding between boron planes, it is somewhat hard to explain the relative strength of titanium diboride along the normal to the basal plane. It would be of great interest if further experimental work could verify to what extent these subtle features in figure 6 are actually present in the electronic charge distribution of TiB_2.

Upon pressure increase to 115 GPa, the charge-density difference at the middle point between in-plane borons increases by about 20%, while the bimodal charge build-up between boron layers grows by 50%. The comparison between the charge-density difference maps at zero pressure and that at 115 GPa, shown in figures 6(c) and 6(d), respectively, can give

some insight into the origin of the rapid increase of both linear bulk moduli B_a and B_c with pressure. Indeed, the main effect of the increasing pressure on the electron distribution in TiB_2 is to promote a charge transfer from the region around the titanium to the vicinity of the boron atoms. This occurs in apparent contradiction with the decrease of the B–B bond-overlap population (see table 7). In fact, the Mulliken population analysis indicates a growing population of the Ti 5sp and 3d valence shells, and that of B 2sp, at the expense of a decrease of the boron diffuse 3sp shell population. However, the charge transferred to the outermost shells of Ti, and to the B 2sp shell, seems to concentrate in the neighbourhood of the boron atoms, with a consequent stiffening of B–B bonds, both those in the plane and those parallel to the c-axis. The net effect of this increase in charge transfer with pressure is the large values found in section 3 for both linear bulk moduli pressure derivatives, B'_{a0} and B'_{c0}. This also helps one to work out how the boron planes in TiB_2 can become stiffer than the carbon planes in graphite at high pressures.

Therefore, the picture that emerges from the analysis of the charge-density distribution in titanium diboride, as calculated within the HF-LCCO approximation, is that the TiB_2 crystal structure can be best viewed as a stacking of interacting boron planes forming cages, inside which rest the titanium atoms. These boron cages are connected together not only along the basal planes, but also, to some extent, along the c-axis. This picture can help one to understand the mechanical properties of titanium diboride, particularly its high hardness and the relative isotropy of its elastic moduli.

6. Conclusions

In this work we were concerned with the structure, equation of state, elastic properties and electronic charge distribution of TiB_2. Our results are in good agreement with the available experimental data, mainly for the lattice parameters. Concerning the TiB_2 bulk modulus, there is a considerable spread in both theoretical and experimental values, as was shown in table 2. Our result ($B_0 = 292$ GPa) seems to be quite reasonable for a hard material such as titanium diboride, and also agrees with the recently measured value for the homologous compound VB_2, whose preliminary analysis points to a value of B_0 around 330 GPa [45].

This work also represents one more test of the suitability of the HF approximation, as implemented in the CRYSTAL95 code, for the description of periodic systems with metallic character [32,46,47]. In fact, the comparison of our results with experiment shows that, despite the lack of any treatment of the electronic correlation, the periodic HF-LCCO approximation provides good estimates for the structural parameters and reasonable values for the elastic moduli of titanium diboride.

The analysis of the charge-density distribution in TiB_2 showed a non-negligible, bimodal excess charge accumulation running along the B–B lines perpendicular to the basal planes. Our results differ qualitatively from the early observations of Will and Kirfel [44], as well as that of van Camp and van Doren [13], and suggest that the electronic charge distribution in titanium diboride should be subjected to further experimental investigation. The main effect of pressure on the electronic density maps is a continuous charge transfer from the neighbourhood of the titanium to a charge envelope developing around boron, and also to the bimodal charge build-up bridging the boron layers, a feature with increasing significance at high pressures.

On the basis of the relative isotropy of the elastic properties of TiB_2 as well as the analysis of its electronic charge-density distribution, we suggest, in accordance with reference [44], that the crystal structure of titanium diboride can be best described as constituted by stacking layers of boron, interacting in a non-negligible way along the c-axis and forming cages, inside which rest the titanium atoms. The metal cores, of course, also contribute to the overall

structural stability, but the direct interaction between borons along the *c*-axis should contribute significantly to the rigidity of the titanium diboride structure. This represents a significant change in the way of thinking about the TiB_2 crystal structure.

Acknowledgments

This work was partially supported by CNPq, FINEP and FAPERGS (Brazil). Some of the calculations were carried out at the Centro Nacional de Supercomputacao da Universidade Federal do Rio Grande do Sul—CESUP. The authors thank Dr J A C Gallas, who gave us access to his own computational resources, and Dr M Towler, for the Unix script shell used to perform the basis-set optimization.

References

[1] Cutler R A 1991 *Engineering Properties of Borides (Engineered Materials Handbook vol 4)* ed S J Schneider Jr *et al* (Metals Park, OH: ASM International)
[2] *The Encyclopedia of Advanced Materials* 1994 vol 1, ed D Bloor, R J Brook, M C Flemings, S Mahajan and R W Cahn (Oxford: Elsevier Science) pp 287–92
[3] Hagen A P (ed) 1991 *Inorganic Reactions and Methods* vol 13, (New York: VCH) p 84–245
[4] *Handbook of Chemistry and Physics* 1989 70th edn, ed R C Weast (Boca Raton, FL: Chemical Rubber Company Press)
[5] Li X, Manghnani M H, Ming L C and Grady D E 1996 *J. Appl. Phys.* **80** 3860
[6] Tian D C and Wang X B 1992 *J. Phys.: Condens. Matter* **4** 8765
[7] Grechnev G E and Ushakova N V 1997 *Low Temp. Phys.* **23** 217
[8] Wang X B, Tian D C and Wang L L 1994 *J. Phys.: Condens. Matter* **6** 10 185
[9] Anishchik V M and Dorozhkin N N 1990 *Phys. Status Solidi* b **160** 173
[10] Armstrong D R 1983 *Theor. Chim. Acta* **64** 137
[11] Burdett J K, Canadell E and Miller G J 1986 *J. Am. Chem. Soc.* **108** 6561
[12] Guillermet A F and Grimvall G 1991 *J. Less-Common Met.* **169** 257
[13] van Camp P E and van Doren V E 1995 *High Pressure Res.* **13** 335
[14] Pere J, Gelizé-Duvignau M and Lichanot A 1999 *J. Phys.: Condens. Matter* **11** 5827
[15] Dovesi R, Saunders V R, Roetti C, Causà M Harrison N M, Orlando R and Aprà E 1996 *CRYSTAL95 User's Manual* University of Torino
[16] Pisani C, Dovesi R and Roetti C 1988 *Hartree–Fock Ab Initio Treatment of Crystalline Systems (Springer Lecture Notes in Chemistry vol 48)* (Heidelberg: Springer)
[17] Saunders V R, unpublished
[18] Causà M and Zupan A 1994 *Chem. Phys. Lett.* **220** 145
[19] Monkhorst H J and Pack J D 1976 *Phys. Rev.* B **13** 5188
[20] Gilat G and Raubenheimer J L 1966 *Phys. Rev.* **144** 390
[21] Press W H, Flannery B P, Teukolsky S A and Vetterling W T 1989 *Numerical Recipes* (Cambridge: Cambridge University Press)
[22] Post B, Glaser F W and Moskowitz D 1954 *Acta Metall.* **2** 20
[23] Hanfland M, Beister H and Syassen K 1989 *Phys. Rev.* B **39** 12 598
[24] Silver A H and Kushida T 1963 *J. Chem. Phys.* **38** 865
[25] Gilman J J and Roberts B W 1961 *J. Appl. Phys.* **32** 1405
[26] Spoor P S, Maynard J D, Pan M J, Green D J, Hellmann J R and Tanaka T 1997 *Appl. Phys. Lett.* **70** 1959
[27] Manghnani M H, Fisher E S, Li F and Grady D E, as discussed in reference [28]
[28] Wright S J 1994 *J. Appl. Crystallogr.* **27** 794
[29] Fast L, Wills J M, Johansson B and Eriksson O 1995 *Phys. Rev.* B **51** 17 431
[30] Catti M, Pavese A, Dovesi R, Roetti C and Causà M 1991 *Phys. Rev.* B **44** 3509
[31] Gale J D, Catlow C R A and Mackrodt W C 1992 *Modell. Simul. Mater. Sci. Eng.* **1** 73
[32] Baraille I, Pouchan C, Causà M and Marinelli F 1998 *J. Phys.: Condens. Matter* **10** 10 969
[33] Nye J F 1964 *Physical Properties of Crystals* (London: Oxford University Press)
[34] Wiley D E, Manning W R and Hunter O Jr 1969 *J. Less-Common Met.* **18** 149
[35] Hill R 1952 *Proc. Phys. Soc.* **65** 349

[36] Gust W H, Holt A C and Royce E B 1973 *J. Appl. Phys.* **44** 550
[37] Abbate A, Frankel J and Dandekar D, as discussed in reference [28]
[38] Grady D E, as discussed in reference [28]
[39] Orlando R, Dovesi R, Roetti C and Saunders V R 1990 *J. Phys.: Condens. Matter* **2** 7769
[40] Szabo A and Ostlund N S 1996 *Modern Quantum Chemistry* (Minneola, FL: Dover) p 152
[41] Mulliken R S 1955 *J. Chem. Phys.* **23** 1833
Mulliken R S 1955 *J. Chem. Phys.* **23** 1841
[42] Kawanowa H, Souda R, Otani S and Gotoh Y 1998 *Phys. Rev. Lett.* **81** 2264
[43] Mizuno M, Tanaka I and Adachi H 1999 *Phys. Rev.* B **59** 15 033
[44] Will G and Kirfel A 1986 *Proc. Int. Conf. on the Physics and Chemistry of Boron and Boron-Rich Borides (Albuquerque, NM, 1985) (AIP Proc. No 140)* (New York: AIP) p 87
[45] Pereira A S, Haines J, Léger J M and da Jornada J A H, unpublished
[46] Dovesi R, Pisani C and Roetti C 1983 *Gazz. Chim. Ital.* **113** 313
[47] Dovesi R, Pisani C, Ricca F and Roetti C 1982 *Phys. Rev.* B **25** 3731